FULL PAPER

Dalton
www.rsc.org/dalton

Complexes of substituted derivatives of 2-(2-pyridyl)benzimidazole with Re(I), Ru(II) and Pt(II): structures, redox and luminescence properties

Nail M. Shavaleev,[a] Zöe R. Bell,[a] Timothy L. Easun,[b] Ramune Rutkaite,[b] Linda Swanson[b] and Michael D. Ward*[a,b]

[a] *School of Chemistry, University of Bristol, Cantock's Close, Bristol, UK BS8 1TS*

[b] *Department of Chemistry, University of Sheffield, Sheffield, UK S3 7HF. E-mail: m.d.ward@sheffield.ac.uk; Fax: +0114 2229346; Tel: +0114 2229484*

Received 23rd July 2004, Accepted 22nd September 2004
First published as an Advance Article on the web 6th October 2004

N,*N*′-Chelating ligands based on the 2-(2-pyridyl)benzimidazole (PB) core have been prepared with a range of substituents (phenyl, pentafluorophenyl, naphthyl, anthracenyl, pyrenyl) connected to the periphery *via* alkylation of the benzimidazolyl unit at one of the N atoms. These PB ligands have been used to prepare a series of complexes of the type [Re(PB)(CO)$_3$Cl], [Pt(PB)(CCR)$_2$] (where –CCR is an acetylide ligand) and [Ru(bpy)$_2$(PB)][PF$_6$]$_2$ (bpy = 2,2′-bipyridine). Six of the complexes have been structurally characterised. Electrochemical and luminescence studies show that all three series of complexes behave in a similar manner to the analogous complexes with 2,2′-bipyridine in place of PB. In particular, all three series of complexes show luminescence in the range 553–605 nm (Pt series), 620–640 nm (Re series) and 626–645 nm (Ru series) arising from the ^{3}MLCT state, with members of the Pt(II) series being the most strongly emissive with lifetimes of up to 500 ns and quantum yields of up to 6% in air-saturated CH_2Cl_2 at room temperature. In the Re and Ru series there was clear evidence for inter-component energy-transfer processes in both directions between the ^{3}MLCT state of the metal centre and the singlet and triplet states of the pendant organic luminophores (naphthalene, pyrene, anthracene). For example the pyrene singlet is almost completely quenched by energy transfer to a Re-based MLCT excited state, which in turn is completely quenched by energy transfer to the lower-lying pyrene triplet state. For the analogous Ru(II) complexes the inter-component energy transfer is less effective, with ^{1}anthracene → Ru(^{3}MLCT) energy transfer being absent, and Ru(^{3}MLCT) → ^{3}anthracene energy transfer being incomplete. This is rationalised on the basis of a greater effective distance for energy transfer in the Ru(II) series, because the MLCT excited states are localised on the bpy ligands which are remote from the pendant aromatic group; in the Re series in contrast, the MLCT excited states involve the PB ligand to which the pendant aromatic group is directly attached, giving more efficient energy transfer.

Introduction

The enormous popularity of metal–bipyridyl complexes showing luminescence from charge-transfer excited states has resulted in the study of many bidentate diimine-type ligands which may show analogous behaviour in their complexes.[1] The opportunities for tuning the steric and electronic properties of the luminescent metal centres using such 'bpy analogues' are huge and the topic of considerable current research.

The *N*,*N*′-diimine chelating ligand 2-(2-pyridyl)benzimidazole (PB) has a venerable history in coordination chemistry.[2,3] Many of the reported complexes of PB have been of interest because of the possibility of deprotonation of the NH group of the imidazole unit, converting the ligand from neutral to anionic forms with different properties.[2,4] Haga showed in [Ru(bpy)$_2$(PB)]$^{2+}$ how the redox and spectroscopic properties of the complex were strongly dependent on pH (protonation/deprotonation of the peripheral NH unit)[4] or, more subtly, on the existence of hydrogen-bonding interactions involving the NH group as donor and N-heterocyclic bases as acceptors.[5] The same group also demonstrated that [Ru(bpy)$_2$(PB)]$^{2+}$ shows ^{3}MLCT luminescence comparable to that of [Ru(bpy)$_3$]$^{2+}$, although slightly red-shifted and with a slightly reduced lifetime.[4]

Ligands based on PB units have more recently been popular in two distinct contexts. First, PB units have been used in the field of self-assembly as components of multinucleating compartmental ligands whose complexes form elaborate molecular architectures such as triple helicates.[6] Secondly, following Haga's initial observation of the luminescence of [Ru(bpy)$_2$(PB)]$^{2+}$,[4] PB derivatives have been used as 'bipyridine analogues' in a variety of complexes with metal ions such as Ru(II), Os(II) and Re(I).[7,8] In particular, functionalisation at the externally directed NH position of PB allows simple incorporation of PB units into multinucleating bridging ligands which contain two or more redox- and photo-active components displaying either ground-state electronic interactions or photoinduced electron- or energy-transfer between sites.[8]

Facile alkylation of the benzimidazole NH group can be used to attach a wide variety of substituents to the metal–diimine core in a way that is not so synthetically convenient for metal–bpy complexes. In this paper accordingly we describe three series of complexes, of Re(I), Ru(II) and Pt(II), with alkylated PB derivatives as ligands; the substituents include aromatic luminophores such as naphthalene, pyrene and anthracene. These complexes are analogues of known luminescent metal–bpy complexes, and we report here their syntheses, some crystal structures, and their luminescence and redox properties.

Experimental

General details

Organic reagents and metal salts were purchased from Aldrich or Avocado and used as received. 2-(2-Pyridyl)benzimidazole,[9] *N*-ethyl-2-(2-pyridyl)benzimidazole[10] (**PBE**) and [Ru(bpy)$_2$Cl$_2$]·2H$_2$O [11] were prepared according to the literature methods. ^{1}H NMR spectra were recorded on a Jeol GX-400 spectrometer, and all mass spectra (FAB and EI) on a VG-Autospec instrument. IR spectra were recorded on a Perkin-Elmer Spectrum One instrument; UV/Vis absorption spectra were recorded on Perkin-Elmer Lambda 2 or Cary 50 spectrometers using CH_2Cl_2 solutions. Steady-state luminescence and excitation

DOI: 10.1039/b411341a

spectra were recorded in aerated CH_2Cl_2 solutions, diluted to give an absorbance of 0.1 or less at the excitation wavelength, on a Perkin-Elmer LS-50 luminescence spectrometer. Luminescence lifetimes were acquired on an Edinburgh Instruments 199 spectrometer operating under single photon counting conditions. The MHz repetition-rate excitation source was either an IBH NanoLED-05 (for 450 nm excitation, used for the Ru complexes) or an IBH NanoLED-03 (for 370 nm excitation, used for the Re and Pt complexes). Fluorescence emission was isolated *via* the use of appropriate narrow band (±10 nm) interference filters (550 or 600 nm, as appropriate). Electrochemical measurements were performed with an EcoChimie Autolab 100 potentiostat, using a conventional three-electrode cell with Pt-wire working and counter electrodes and an Ag/AgCl reference electrode. Ferrocene was used in each experiment as an internal standard and all potentials are quoted with respect to the ferrocene–ferrocenium couple.

Procedure for preparation of ligands

Dry 2-(2-pyridyl)benzimidazole (1.5 g, 7.7 mmol) was added to a suspension of NaH (0.62 g, 26 mmol) in dry DMF (30 cm^3) under N_2 and stirred for 30 min at room temperature. NaH was used as a 60% suspension in mineral oil and was washed with dry degassed hexane before the reaction to remove the oil. A slight excess of the appropriate bromo- or chloromethyl derivative (8–9 mmol) was added to the resulting suspension and the mixture was heated at 100 °C for 24 h. The reaction mixture was cooled down and poured into water (200 cm^3). The precipitate formed was collected by filtration, dissolved in CH_2Cl_2, dried with $MgSO_4$, reduced in volume and purified by column chromatography on silica eluting with MeOH–CH_2Cl_2 (0/100 to 2/98) or on alumina eluting with CH_2Cl_2. The blue-luminescent fraction containing the product was reduced in volume and ethanol was added to it. The CH_2Cl_2 was evaporated to give a suspension of the product in ethanol that was filtered off, washed with ethanol and hexane, and dried to give pure product in reasonable yield.

Data for PBPh. Alkylating agent: benzyl bromide (1.1 cm^3, 1.58 g, 9.2 mmol); yield 1.46 g (67%). Anal. Calc. for $C_{19}H_{15}N_3$: C, 80.0; H, 5.3; N, 14.7. Found: C, 80.2; H, 5.5; N, 14.8%. EIMS: *m*/*z* 284 (100% $\{M\}^+$). λ_{max}/nm (ε/M^{-1} cm^{-1}): 311 (21600).

Data for PBF. Alkylating agent: 2,3,4,5,6-pentafluorobenzyl bromide (1.3 cm^3, 2.25 g, 8.6 mmol); yield 2.05 g (71%). Anal. Calc. for $C_{19}H_{10}N_3F_5$: C, 60.8; H, 2.7; N, 11.2. Found: C, 61.3; H, 2.7; N, 11.4%. EIMS: *m*/*z* 375 (90% $\{M\}^+$), 356 (100% $\{M - F\}^+$). λ_{max}/nm (ε/M^{-1} cm^{-1}): 310 (22200). ^{1}H NMR (CD_2Cl_2): δ 8.64 (1H, d, *J* 4; pyridyl H6), 8.42 (1H, d, *J* 8; pyridyl H3), 7.89 (1H, td, *J* 8, 1.6; pyridyl H4), 7.78 (1H, m; pyridyl H5), 7.35–7.44 (2H, m; benzimidazolyl C_6H_4), 7.31 (2H, m; benzimidazolyl C_6H_4), 6.44 (2H, s; CH_2).

Data for PBN. Alkylating agent: 2-bromomethylnaphthalene (1.80 g, 8.1 mmol); yield 0.85 g (33%). Anal. Calc. for $C_{23}H_{17}N_3$: C, 82.4; H, 5.1; N, 12.5. Found: C, 82.3; H, 5.2; N, 12.7%. EIMS: *m*/*z* 335 (100%, M^+). λ_{max}/nm (ε/M^{-1} cm^{-1}): 311 (22600). ^{1}H NMR (CD_2Cl_2): δ 8.62 (1H, d, *J* 5; pyridyl H^6), 8.46 (1H, d, *J* 8; pyridyl H^3), 7.86 (1H, td, *J* 8, 1.6; pyridyl H^4), 7.72–7.82 (3H, m; pyridyl H^5 and 2 naphthyl), 7.68 (1H, m; naphthyl), 7.56 (1H, s; naphthyl), 7.2–7.45 (7H, m; 3 naphthyl CH and 4 benzimidazolyl CH), 6.36 (2H, s; CH_2).

Data for PBA. Alkylating agent: 9-chloromethylanthracene (1.74 g, 7.7 mmol); yield 1.61 g (54%). Anal. Calc. for $C_{27}H_{19}N_3$: C, 84.1; H, 5.0; N, 10.9. Found: C, 83.2; H, 4.7; N, 10.3%. EIMS: *m*/*z* 385 (80%, M^+). λ_{max}/nm (ε/M^{-1} cm^{-1}): 390 (9500), 370 (10100), 351 (6700), 308 (19500), 258 (166000). ^{1}H NMR (CD_2Cl_2): δ 8.74 (1H, d, *J* 4; pyridyl H^6), 8.54 (1H, s; anthracenyl H^{10}), 8.42–8.5 (3H, m; pyridyl H^3 and 2 anthracenyl CH), 8.07 (2H, m; 2 anthacenyl CH), 7.96 (1H, td, *J* 8, 1.6; pyridyl H^4), 7.64 (1H, d, *J* 8; pyridyl H^3), 7.4–7.5 (5H, m; 4 benzimidazolyl CH and anthracenyl CH); 7.25 (2H, s; CH_2), 7.01 (1H, t, *J* 8; anthracenyl CH), 6.64 (1H, t, *J* 8; anthracenyl CH), 6.27 (1H, d, *J* 8; anthracenyl CH).

Data for PBPyr. Alkylating agent: bromomethylpyrene (2.33 g, 7.9 mmol); yield 1.73 g, 55%). Anal. Calc. for $C_{29}H_{19}N_3$: C, 85.1; H, 4.7; N, 10.3. Found: C, 84.5; H, 4.7; N, 10.0%. EIMS: *m*/*z* 409 (85%, M^+). λ_{max}/nm (ε/M^{-1} cm^{-1}): 346 (45000), 329 (42400), 314 (33900), 278 (47700), 267 (29500), 244 (70300). ^{1}H NMR (CD_2Cl_2): δ 8.48–8.55 (2H, m; 2 × pyrene CH), 8.42 (1H, d, *J* 5; pyridyl H^6), 8.2–8.3 (3H, m; pyridyl H^3 and 2 × pyrene CH), 8.04–8.1 (2H, m; 2 × pyrene CH), 7.92–8.0 (2H, m; 2 × pyrene CH), 7.87 (1H, d, *J* 8; pyrene CH), 7.83 (1H, td, *J* 8, 1.5; pyridyl H^4), 7.15–7.35 (5H, m; 4 benzimidazolyl CH and pyridyl H^5), 6.99 (2H, s; CH_2).

Preparations of Re(I) complexes

A mixture of $Re(CO)_5Cl$ and the appropriate ligand in a 1 : 1 molar ratio was heated to reflux in dry, degassed toluene (30 cm^3) under N_2 for 24 h and then cooled down to room temperature. The resulting yellow/orange precipitate was filtered off, and washed with hexane and ether. The precipitate was dissolved in CH_2Cl_2, hexane was added to the solution, the CH_2Cl_2 was removed under reduced pressure. The resulting suspension of the target complex in hexane was filtered off, washed with hexane and ether and dried under vacuum. All complexes are air- and moisture-stable yellow solids generally soluble in chlorinated solvents, THF, and acetone, but insoluble in hexane and ether. It should be noted that attempted column chromatography of the complexes on alumina eluting with CH_2Cl_2 was not successful.

Data for Re–PBPh. Yield: 86%. Anal. Calc. for $C_{22}H_{15}ClN_3O_3Re$: C, 44.7; H, 2.6; N, 7.1. Found: C, 44.7; H, 2.3; N, 7.1%. FABMS: *m*/*z* 614 (14% $\{M + Na\}^+$), 591 (60% $\{M\}^+$), 563 (23% $\{M - CO\}^+$), 556 (100% $\{M - Cl\}^+$), 535 (16% $\{M - 2CO\}^+$). IR (CH_2Cl_2/cm^{-1}): 2022, 1917, 1895. X-Ray quality crystals were grown by slow evaporation of a CH_2Cl_2/heptane solution of the complex.

Data for Re–PBN. Yield: 90%. Anal. Calc. for $C_{26}H_{17}ClN_3O_3Re$: C, 48.7; H, 2.7; N, 6.6. Found: C, 48.5; H, 2.6; N, 6.5%. FABMS: *m*/*z* 641 (12%, $\{M\}^+$), 613 (6% $\{M - CO\}^+$), 606 (22% $\{M - Cl\}^+$). IR (CH_2Cl_2/cm^{-1}): 2022, 1917, 1895.

Data for Re–PBA. Yield: 72%. Anal. Calc. for $C_{30}H_{19}ClN_3O_3Re$: C, 52.1; H, 2.8; N, 6.1. Found: C, 51.5; H, 2.0; N, 6.2%. FABMS: *m*/*z* 691 (6% $\{M\}^+$), 656 (7% $\{M - Cl\}^+$). IR (CH_2Cl_2/cm^{-1}): 2022, 1917, 1895.

Data for Re–PBF. Yield: 70%. Anal. Calc. for $C_{22}H_{10}ClF_5N_3O_3Re$: C, 38.8; H, 1.5; N, 6.2. Found: C, 39.1; H, 1.3; N, 6.2%. FABMS: *m*/*z* 704 (15% $\{M + Na\}^+$), 681 (60%, M^+), 646 (100% $\{M - Cl\}^+$), 625 (20% $\{M - 2CO\}^+$), 597 (10% $\{M - 3CO\}^+$). IR (CH_2Cl_2/cm^{-1}): 2023, 1918, 1897. X-Ray quality crystals were grown by slow evaporation of a THF–heptane solution of the complex.

Data for Re–PBPyr. Yield: 84%. Anal. Calc. for $C_{32}H_{19}ClN_3O_3Re$: C, 53.7; H, 2.7; N, 5.9. Found: C, 54.0; H, 2.6; N, 6.1%. FABMS: *m*/*z* 715 (8%, M^+), 680 (7% $\{M - Cl\}^+$). IR (CH_2Cl_2/cm^{-1}): 2022, 1917, 1895. X-Ray quality crystals were grown by slow evaporation of THF/heptane solution of the complex.

Preparations of Ru(II) complexes

A mixture of $[Ru(bpy)_2Cl_2]\cdot 2H_2O$ (100 mg, 0.19 mmol) and the appropriate ligand (0.2 mmol) was heated to reflux in degassed

ethanol (30 cm^3) under N_2 for 24 h to give a clear red solution. A few drops of a saturated aqueous solution of KNO_3 were added to the solution and the resulting mixture was evaporated; the solid residue was dissolved in CH_3CN, loaded on to a silica column and eluted with KNO_3 (saturated aqueous solution)–H_2O–CH_3CN starting with the ratio 1.5 : 4 : 200 and slowly increasing the polarity by increasing the proportions of water and saturated aqueous KNO_3 relative to MeCN. The main red fraction was collected, evaporated to dryness and re-dissolved in a small amount of CH_3CN. The excess of KNO_3 was filtered off and the filtrate was evaporated to dryness, dissolved in water (adding a few drops of CH_3CN if necessary) and the product was precipitated by the addition of an aqueous solution of KPF_6. The product was filtered off, washed with water and ether, and dried under vacuum.

Data for Ru–PBN. Yield: 42%. Anal. Calc. for $C_{43}H_{33}F_{12}N_7P_2Ru$: C, 49.7; H, 3.2; N, 9.4. Found: C, 49.2; H, 3.1; N, 9.1%. FABMS: *m*/*z* 894 (100% $\{M - PF_6\}^+$), 608 (85% $\{M - 2PF_6 - CH_2naphthyl\}^+$).

Data for Ru–PBF. Yield: 46%. Anal. Calc. for $C_{39}H_{26}F_{17}N_7P_2Ru$: C, 43.4; H, 2.4; N, 9.1. Found: C, 42.8; H, 2.3; N, 8.9%. FABMS: *m*/*z* 934 (100% $\{M - PF_6\}^+$), 608 (75% $\{M - 2PF_6 - CH_2C_6F_5\}^+$).

Data for Ru–PBA. Yield: 62%. Anal. Calc. for $C_{47}H_{35}F_{12}N_7P_2Ru$: C, 51.9; H, 3.2; N, 9.0. Found: C, 51.4; H, 3.2; N, 8.9%. FABMS: *m*/*z* 1112 (2% $\{M + Na\}^+$), 944 (40% $\{M - PF_6\}^+$), 608 (100% $\{M - 2PF_6 - CH_2anthracenyl\}^+$). X-Ray quality crystals were grown by slow evaporation of an acetone–heptane solution of the complex.

Data for Ru–PBPyr. Yield: 81%. Anal. Calc. for $C_{49}H_{35}F_{12}N_7P_2Ru$: C, 52.9; H, 3.2; N, 8.8. Found: C, 52.7; H, 3.1; N, 8.5%. FABMS: *m*/*z* 968 (40% $\{M - PF_6\}^+$), 608 (100% $\{M - 2PF_6 - CH_2pyrenyl\}^+$).

Preparations of Pt(II) complexes

These were prepared in two steps: first the ligand (L) is reacted with $Pt(DMSO)_2Cl_2$ to give $PtLCl_2$; the dichloride is then converted to the diacetylide $PtL(CCR)_2$ in a separate step.

Preparation of the dichloride intermediates

A mixture of $Pt(DMSO)_2Cl_2$ (0.21 g, 0.5 mmol) and the appropriate ligand (1 equivalent) in degassed acetonitrile (30 cm^3) was refluxed under N_2 for 24 h. The reaction mixture was then cooled to 0 °C and the resulting yellow precipitate was filtered off, and washed with hexane and ether. All complexes are air- and moisture-stable yellow solids which are generally insoluble in organic solvents. The complexes show yellow/orange luminescence in the solid state.

Data for $Pt(PBE)Cl_2$. Yield: 85%. Anal. Calc. for $C_{14}H_{13}Cl_2N_3Pt$: C, 34.4; H, 2.7; N, 8.6. Found: C, 34.8; H, 2.4; N, 8.3%.

Data for $Pt(PBPh)Cl_2$. Yield: 87%. Anal. Calc. for $C_{19}H_{15}Cl_2N_3Pt$: C, 41.4; H, 2.7; N, 7.6. Found: C, 41.7; H, 2.3; N, 7.1%. FABMS: *m*/*z* 574 (4% $\{M + Na\}^+$); 516 (10% $\{M - Cl\}^+$).

Data for $Pt(PBF)Cl_2$. Yield: 91%. Anal. Calc. for $C_{19}H_{10}F_5Cl_2N_3Pt$: C, 35.6; H, 1.6; N, 6.6. Found: C, 36.1; H, 1.5; N, 6.6%.

Data for $Pt(PBN)Cl_2$. Yield: 98%. Anal. Calc. for $C_{23}H_{17}Cl_2N_3Pt$: C, 45.9; H, 2.9; N, 7.0. Found: C, 46.4; H, 3.1; N, 7.4%.

Preparation of the diacetylide complexes

A mixture of the appropriate platinum(II) chloride complex (0.2 mmol), anhydrous CuI (7 mg, catalyst), and dry iPr_2NH (2 cm^3) in dry, degassed dichloromethane (30 cm^3) under N_2 was stirred for 10 min, followed by addition of the appropriate acetylene (10-fold excess). The resulting suspension was stirred under N_2 at room temperature protected from light for 2–5 days. The reaction mixture could be sonicated in a small ultrasound cleaning bath to facilitate the reaction. By the end of reaction the suspension had dissolved to give a yellow/red solution from which the solvent was evaporated. The solid residue was dried under vacuum to remove traces of iPr_2NH and the product purified by column chromatography on alumina, eluting with CH_2Cl_2 unless stated otherwise. The fraction containing the product was collected and reduced in volume to 5 cm^3. The complex was then precipitated by addition of hexane, filtered off, washed with hexane and ether, and dried under vacuum. All of the Pt(II)–diacetylide complexes are air- and moisture-stable solids of yellow/orange colour which are soluble in CH_2Cl_2, acetone and tetrahydrofuran, and insoluble in ether and hexane.

Data for Pt–PBE–Ph. Yield: 76%. Anal. Calc. for $C_{30}H_{23}N_3Pt$: C, 58.1; H, 3.7; N, 6.8. Found: C, 57.9; H, 3.5; N, 6.6%. FABMS: *m*/*z* 621 (32% $\{M\}^+$). X-Ray quality crystals were grown by slow evaporation of a CH_2Cl_2–heptane solution of the complex.

Data for Pt–PBE–CF_3. Yield: 82%. Anal. Calc. for $C_{32}H_{21}F_6N_3Pt$: C, 50.8; H, 2.8; N, 5.6. Found: C, 51.0; H, 2.5; N, 5.3%. FABMS: *m*/*z* 757 (16% $\{M\}^+$).

Data for Pt–PBPh–Ph. Yield: 47%. Anal. Calc. for $C_{35}H_{25}N_3Pt$: C, 61.6; H, 3.7; N, 6.2. Found: C, 61.5; H, 3.7; N, 6.4%. FABMS: *m*/*z* 682 (14% $\{M\}^+$).

Data for Pt–PBPh–CF_3. Yield: 78%. Anal. Calc. for $C_{37}H_{23}F_6N_3Pt$: C, 54.3; H, 2.8; N, 5.1. Found: C, 54.9; H, 2.9; N, 5.3%. FABMS: *m*/*z* 841 (4% $\{M + Na\}^+$), 819 (40% $\{M\}^+$).

Data for Pt–PBPh–Py. Yield: 60%. Anal. Calc. for $C_{33}H_{23}N_5Pt$: C, 57.9; H, 3.4; N, 10.2. Found: C, 58.2; H, 3.1; N, 10.2%. FABMS: *m*/*z* 707 (42% $\{M + Na\}^+$), 685 (100% $\{M\}^+$). X-Ray quality crystals were grown by slow evaporation of THF–heptane solution of the complex.

Data for Pt–PBF–Ph. Yield: 64%. Anal. Calc. for $C_{35}H_{20}F_5N_3Pt$: C, 54.4; H, 2.6; N, 5.4. Found: C, 54.6; H, 2.8; N, 5.6%. FABMS: *m*/*z* 771 (27% $\{M\}^+$).

Data for Pt–PBN–Ph. Yield: 83%. Anal. Calc. for $C_{39}H_{27}N_3Pt$: C, 63.9; H, 3.7; N, 5.7. Found: C, 63.8; H, 3.5; N, 5.6%. FABMS: *m*/*z* 755 (15% $\{M + Na\}^+$), 733 (70% $\{M\}^+$).

X-Ray crystallography

For each complex a suitable crystal was coated with hydrocarbon oil and attached to the tip of a glass fibre, which was then transferred to a Bruker-AXS SMART diffractometer under a stream of cold N_2. Details of the crystal parameters, data collection and refinement for each of the structures are collected in Table 1. After data collection, in each case an empirical absorption correction (SADABS) was applied,[12] and the structures were then solved by conventional direct methods and refined on all F^2 data using the SHELX suite of programs.[13] In all cases non-hydrogen atoms were refined with anisotropic thermal parameters; hydrogen atoms were included in calculated positions and refined with isotropic thermal parameters.

Refinement of the structure of **Pt–PBE–Ph** proceeded without any problems. For **Re–PBF**, **Pt–PBPh–Py** and **Re–PBPyr**·thf, the 'squeeze' command was used to eliminate residual electron density peaks which presumably corresponded to highly disordered solvent molecules which could not be properly identified or refined; in **Re–PBPyr**·thf the thermal parameters for the lattice thf molecule that could be located are rather large. In **Re–PBPh**·CH_2Cl_2 the atoms C(51), C(61) and C(16) were refined with isotropic thermal parameters to keep the

Table 1 Crystal, data collection and refinement details for the crystal structures[a]

Complex	**Ru–PBA**·Me_2CO	**Re–PBPh**·CH_2Cl_2	**Re–PBF**	**Re–PBPyr**·thf	**Pt–PBPh–py**	**Pt–PBE–Ph**
Formula	$C_{50}H_{41}F_{12}N_7OP_2Ru$	$C_{23}H_{17}Cl_3N_3O_3Re$	$C_{22}H_{10}ClF_5N_3O_3Re$	$C_{36}H_{27}ClN_3O_4Re$	$C_{33}H_{23}N_5Pt$	$C_{30}H_{23}N_3Pt$
M_r	1146.91	675.95	680.98	787.26	684.65	620.60
Crystal system	Monoclinic	Orthorhombic	Triclinic	Triclinic	Monoclinic	Monoclinic
Space group	$P2_1/n$	$Pca2_1$	$P\bar{1}$	$P\bar{1}$	$P2_1/c$	$P2_1/n$
T/K	173	100	173	173	173	173
a/Å	22.253(7)	8.908(3)	9.3838(15)	12.055(2)	12.2261(14)	13.435(4)
b/Å	8.776(3)	12.523(4)	12.105(2)	12.376(3)	12.0913(19)	7.5867(13)
c/Å	26.835(13)	20.764(5)	12.532(2)	13.047(2)	22.271(3)	23.436(5)
α/°	90	90	99.044(15)	108.288(14)	90	90
β/°	113.88(2)	90	111.359(17)	100.199(15)	99.635(12)	105.215(14)
γ/°	90	90	91.924(17)	99.195(13)	90	90
V/Å^3	4792(3)	2316.3(11)	1302.8(4)	1770.0(6)	3245.8(8)	2305.0(10)
Z	4	4	2	2	4	4
D_c/g cm^{-3}	1.590	1.938	1.736	1.477	1.401	1.788
Crystal size/mm	0.3 × 0.1 × 0.05	0.5 × 0.15 × 0.15	0.5 × 0.2 × 0.2	0.4 × 0.2 × 0.2	0.5 × 0.5 × 0.4	0.4 × 0.2 × 0.05
μ/mm^{-1}	0.488	5.624	4.828	3.548	4.349	6.112
Data, restraints, parameters	8428, 84, 660	5208, 1, 283	5904, 0, 316	8044, 0, 406	7426, 0, 352	5140, 0, 308
Final $R1$, $wR2$	0.0721, 0.1930	0.0403, 0.0876	0.0223, 0.0514	0.0284, 0.0668	0.0290, 0.0744	0.0355, 0.0763

[a] All data sets were collected on a Bruker SMART diffractometer with Mo-Kα radiation (λ = 0.71073 Å, 2θ limit 55°).

refinement stable as the data was weak. For **Ru–PBA**·Me_2CO the thermal parameters of the F atoms of the hexafluorophosphate anions were refined with isotropic restraints, apart from atoms F(11) and F(12) which needed to be refined with isotropic thermal parameters.

CCDC reference numbers 245715–245720.

See http://www.rsc.org/suppdata/dt/b4/b411341a/ for crystallographic data in CIF or other electronic format.

Results and discussion

Syntheses and structures of complexes

The ligands (Scheme 1) were readily prepared by alkylation of the parent compound **PB** with appropriate halomethyl compounds in DMF using NaH as base. Yields were respectable and all ligands were fully characterised by the usual techniques (see Experimental section for details).

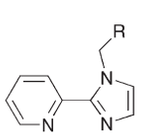

PBE (R = Me; see Fig. 5)
PBPh (R = Ph; see Figs. 1, 6)
PBF (R = C_6F_5; see Fig. 2)
PBN (R = 2-naphthyl)
PBA (R = 9-anthracenyl; see Fig. 4)
PBPyr (R = 1-pyrenyl; see Fig. 3)

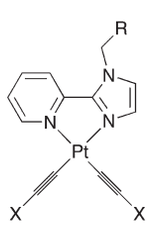

Pt-PBPh-CF$_3$ (R = Ph, X = *p*-$C_6H_4CF_3$)
Pt-PBE-Ph (R = Me, X = Ph)
Pt-PBPh-Py (R = Ph, X = 2-pyridyl)
Pt-PBN-Ph (R = 2-naphthyl, X = Ph)

etc.

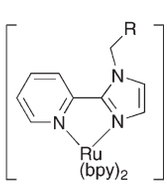

$(PF_6)_2$

Ru-PBE (R = Me)

etc.

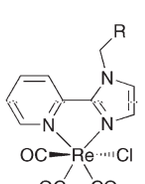

Re-PBE (R = Me)

etc.

Scheme 1

The metal complexes (Scheme 1) were prepared using standard methods, as for related metal-diimine complexes. Thus, reaction of a pyridylbenzimidazole ligand L with $Re(CO)_5Cl$ in toluene at reflux afforded $Re(CO)_3ClL$; reaction with $Ru(bpy)_2Cl_2$ in ethanol at reflux, followed by anion metathesis, afforded $[Ru(bpy)_2L][PF_6]_2$; and reaction with $Pt(dmso)_2Cl_2$ afforded intermediates $PtLCl_2$, which were further reacted with an acetylene RCCH in the presence of CuI and diisopropylamine to give the ultimate products $PtL(CCR)_2$. All complexes provided satisfactory analytical and mass spectroscopic data, and several have been structurally characterised (Figs. 1–6; see also Tables 1 and 2, for crystallographic data and selected structural parameters, respectively).

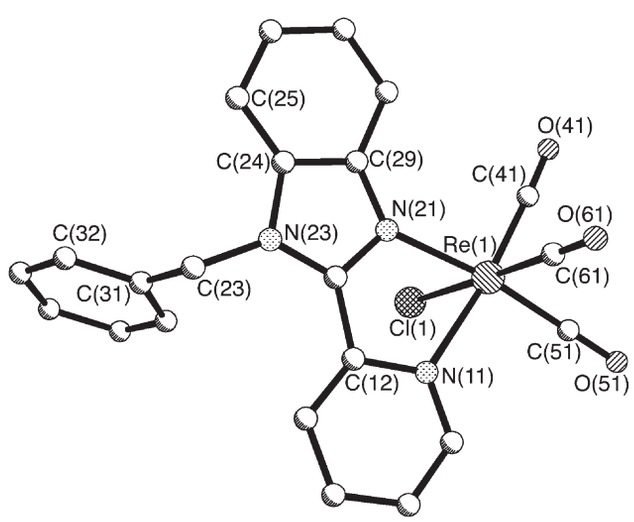

Fig. 1 Molecular structure of **Re–PBPh**.

The Re(I) complexes **Re–PBPh**, **Re–PBF** and **Re–PBPyr** (Figs. 1–3) all have very similar coordination geometries about the metal centre, with a *fac*-tricarbonyl disposition of ligands and a near-octahedral geometry typical of Re(I)–diimine–tricarbonyl complexes of this type.[14] The Re–N distance to the benzimidazole ring is slightly shorter than that to the pyridyl donor, as was observed recently for **Re–PBE**.[7b] The bite angles of the chelating PB ligands are close to 74° in every case; the ligands are not completely planar, with small twists between the pyridyl and benzimidazolyl components, of *ca.* 2.5° in **Re–PBF**; 10° in **Re–PBPyr**; and 5° in **Re–PBPh**. The C–O distances lie

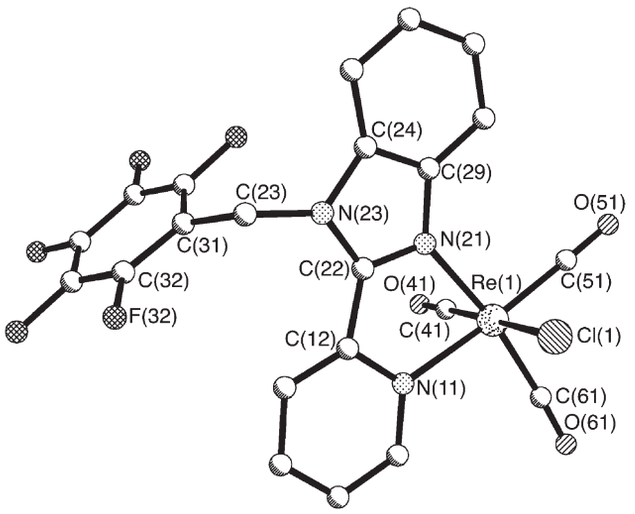

Fig. 2 Molecular structure of **Re–PBF**.

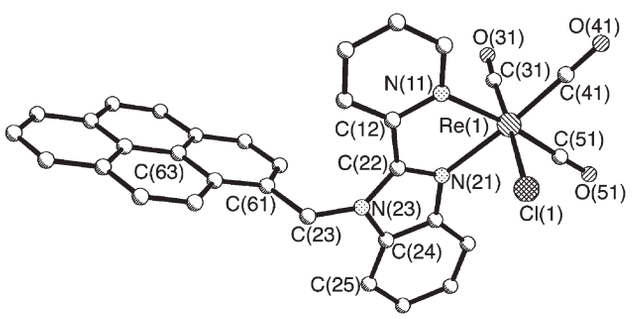

Fig. 3 Molecular structure of **Re–PBPyr**.

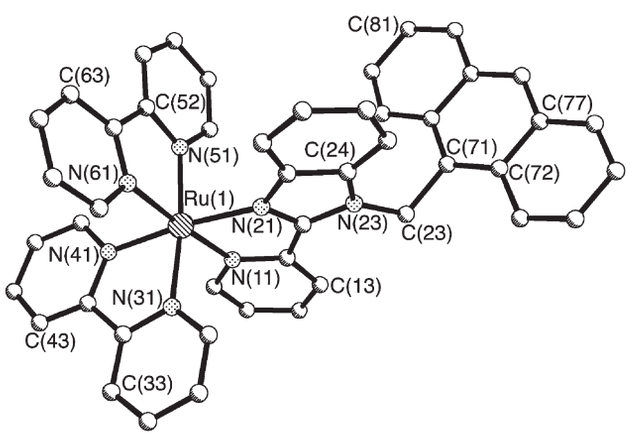

Fig. 4 Molecular structure of the complex cation of **Ru–PBA**.

in the range 1.11–1.17 Å. Partial localisation of single and double bonds in the imidazole unit is clear, as the structure of **Re–PBF** illustrates: the N(21)–C(22) distance of 1.325(4) Å, formally the C=N bond, is the shortest distance within the five-membered imidazole ring. All other bond distances within this ring, and also within the pyridyl ring, lie in the range 1.35–1.40 Å; in contrast, the formally single bond between the rings, C(12)–C(22), has a distance of 1.471 Å. The same general pattern occurs in the structures of **Re–PBPh** and **Re–PBPyr**. In all three cases, the aromatic unit pendant from the benzimidazole group is almost perpendicular to the benzimidazole mean plane, with the mean plane of the substituent making an angle of 74.6, 87.6 and 88.4° with the benzimidazole plane for **Re–PBPh**, **Re–PBF** and **Re–PBPyr**, respectively.

Ru–PBA (Fig. 4) likewise has a typical pseudo-octahedral geometry with bond distances and angles in the normal range for Ru(II)–diimine complexes; the Ru–N separations lie in the range 2.041(7)–2.084(7) Å, *cf.* 2.06 Å for $[Ru(bpy)_3]^{2+}$.[15] Again, the Ru–N(benzimidazole) distance [2.057(7) Å] is

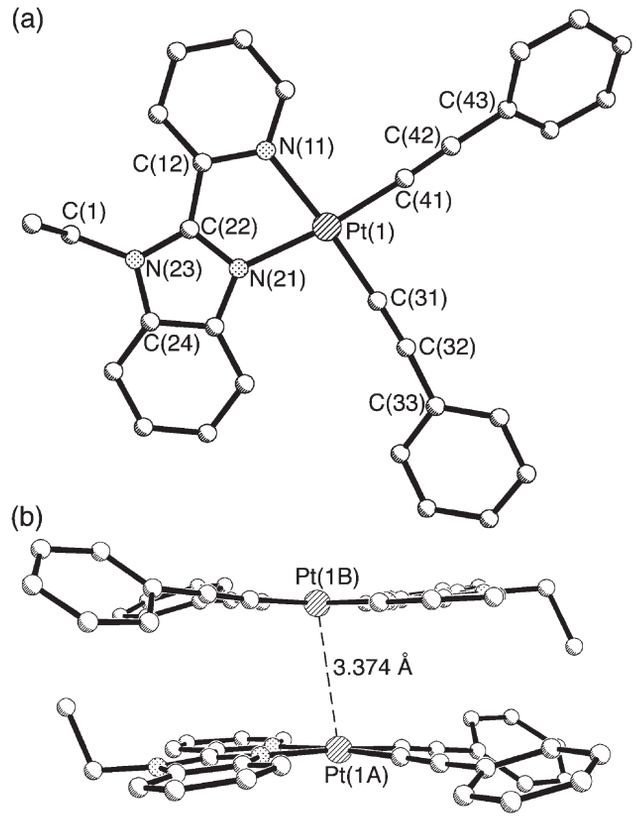

Fig. 5 Molecular structure of **Pt–PBE–Ph**.

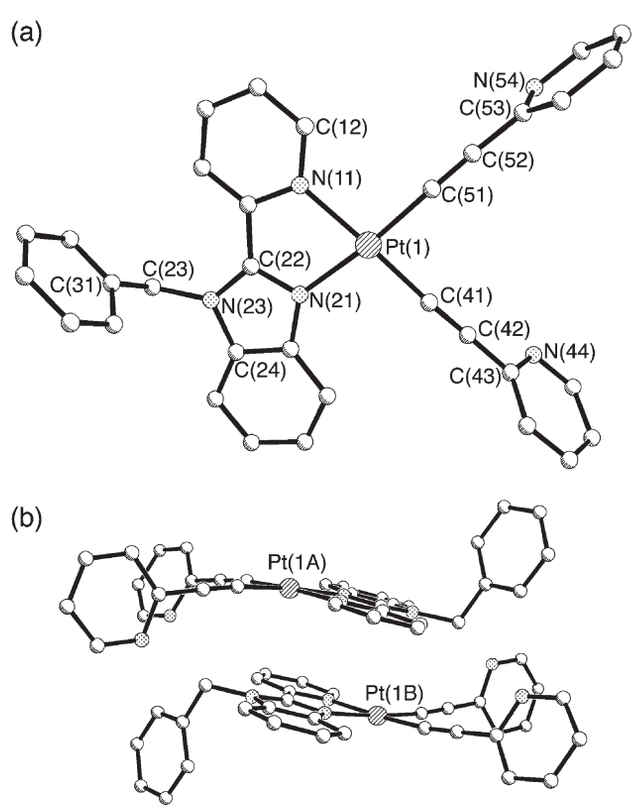

Fig. 6 Molecular structure of **Pt–PBPh–Py**.

slightly shorter than the Ru–N(pyridyl) distance [2.084(7) Å]; the chelating bite angle of the PBA ligand is 77°, and the twist between the two components of this ligand is 12°. The partial localisation of bonds within the five-membered imidazole ring is apparent, with the double bond N(21)–C(22) being the shortest of all bonds in the ligand, at 1.32(1) Å. The mean plane of the anthracene unit is inclined at 87.5° to the mean plane of the benzimidazole unit.

Table 2 Selected bond distances (Å) and angles (°) for the six structures

Ru–PBA·Me_2CO

Ru(1)–N(51)	2.040(8)	Ru(1)–N(61)	2.061(8)
Ru(1)–N(41)	2.056(8)	Ru(1)–N(21)	2.061(7)
Ru(1)–N(31)	2.059(9)	Ru(1)–N(11)	2.082(7)
N(51)–Ru(1)–N(41)	97.1(3)	N(31)–Ru(1)–N(21)	98.0(3)
N(51)–Ru(1)–N(31)	173.1(3)	N(61)–Ru(1)–N(21)	101.3(3)
N(41)–Ru(1)–N(31)	78.6(4)	N(51)–Ru(1)–N(11)	97.8(3)
N(51)–Ru(1)–N(61)	78.3(3)	N(41)–Ru(1)–N(11)	96.1(3)
N(41)–Ru(1)–N(61)	85.7(3)	N(31)–Ru(1)–N(11)	88.1(3)
N(31)–Ru(1)–N(61)	95.9(3)	N(61)–Ru(1)–N(11)	175.9(3)
N(51)–Ru(1)–N(21)	86.9(3)	N(21)–Ru(1)–N(11)	77.1(3)
N(41)–Ru(1)–N(21)	172.6(3)		

Re–PBPh·CH_2Cl_2

Re(1)–C(41)	1.910(7)	Re(1)–N(21)	2.159(6)
Re(1)–C(51)	1.919(7)	Re(1)–N(11)	2.218(7)
Re(1)–C(61)	1.930(8)	Re(1)–Cl(1)	2.4786(19)
C(41)–Re(1)–C(51)	87.2(3)	C(61)–Re(1)–N(11)	96.0(3)
C(41)–Re(1)–C(61)	87.8(3)	N(21)–Re(1)–N(11)	74.4(2)
C(51)-Re(1)–C(61)	87.9(3)	C(41)–Re(1)–Cl(1)	93.0(2)
C(41)–Re(1)–N(21)	100.3(3)	C(51)–Re(1)–Cl(1)	94.48(19)
C(51)–Re(1)–N(21)	172.2(2)	C(61)–Re(1)–Cl(1)	177.5(2)
C(61)–Re(1)–N(21)	94.2(3)	N(21)–Re(1)–Cl(1)	83.31(16)
C(41)–Re(1)–N(11)	173.7(3)	N(11)–Re(1)–Cl(1)	82.91(18)
C(51)–Re(1)–N(11)	97.9(2)		

Re–PBF

Re(1)–C(41)	1.901(3)	Re(1)–N(21)	2.161(2)
Re(1)–C(61)	1.910(3)	Re(1)–N(11)	2.189(3)
Re(1)–C(51)	1.926(3)	Re(1)–Cl(1)	2.4960(8)
C(41)–Re(1)–C(61)	88.23(13)	C(51)–Re(1)–N(11)	174.70(11)
C(41)–Re(1)–C(51)	90.22(13)	N(21)–Re(1)–N(11)	73.82(9)
C(61)–Re(1)–C(51)	88.90(13)	C(41)–Re(1)–Cl(1)	176.26(9)
C(41)–Re(1)–N(21)	95.05(11)	C(61)–Re(1)–Cl(1)	94.06(9)
C(61)–Re(1)–N(21)	169.41(10)	C(51)–Re(1)–Cl(1)	92.78(9)
C(51)–Re(1)–N(21)	101.13(12)	N(21)–Re(1)–Cl(1)	82.18(6)
C(41)–Re(1)–N(11)	91.82(11)	N(11)–Re(1)–Cl(1)	85.00(7)
C(61)–Re(1)–N(11)	96.06(11)		

Re–PBPyr·thf

Re(1)–C(31)	1.913(4)	Re(1)–N(21)	2.166(3)
Re(1)–C(51)	1.920(4)	Re(1)–N(11)	2.201(3)
Re(1)–C(41)	1.925(4)	Re(1)–Cl(1)	2.4868(9)
C(31)–Re(1)–C(51)	87.52(16)	C(41)–Re(1)–N(11)	98.31(15)
C(31)–Re(1)–C(41)	88.52(15)	N(21)–Re(1)–N(11)	73.82(10)
C(51)–Re(1)–C(41)	87.48(17)	C(31)–Re(1)–Cl(1)	177.53(12)
C(31)–Re(1)–N(21)	94.77(13)	C(51)–Re(1)–Cl(1)	94.37(11)
C(51)–Re(1)–N(21)	100.32(13)	C(41)–Re(1)–Cl(1)	93.15(11)
C(41)–Re(1)–N(21)	171.64(14)	N(21)–Re(1)–Cl(1)	83.33(7)
C(31)–Re(1)–N(11)	93.93(14)	N(11)–Re(1)–Cl(1)	84.03(7)
C(51)–Re(1)–N(11)	174.06(12)		

Pt–PBPh–Py

Pt(1)–C(41)	1.947(4)	C(41)–C(42)	1.220(5)
Pt(1)–C(51)	1.958(4)	C(42)–C(43)	1.428(6)
Pt(1)–N(21)	2.062(3)	C(51)–C(52)	1.205(5)
Pt(1)–N(11)	2.075(3)	C(52)–C(53)	1.427(5)
C(41)–Pt(1)–C(51)	86.08(16)	N(21)–Pt(1)–N(11)	77.91(12)
C(41)–Pt(1)–N(21)	98.68(14)	C(42)–C(41)–Pt(1)	174.0(3)
C(51)–Pt(1)–N(21)	173.91(14)	C(41)–C(42)–C(43)	178.1(4)
C(41)–Pt(1)–N(11)	175.08(13)	C(52)–C(51)–Pt(1)	174.1(3)
C(51)–Pt(1)–N(11)	97.10(14)	C(51)–C(52)–C(53)	176.6(4)

Pt–PBE–Ph

Pt(1)–C(31)	1.942(5)	C(31)–C(32)	1.207(7)
Pt(1)–C(41)	1.950(5)	C(32)–C(33)	1.450(7)
Pt(1)–N(21)	2.070(4)	C(41)–C(42)	1.210(7)
Pt(1)–N(11)	2.079(4)	C(42)–C(43)	1.440(7)

Table 2 (*Contd.*)

Pt–PBE–Ph

C(31)–Pt(1)–C(41)	88.6(2)	N(21)–Pt(1)–N(11)	77.77(16)
C(31)–Pt(1)–N(21)	97.88(18)	C(32)–C(31)–Pt(1)	177.4(5)
C(41)–Pt(1)–N(21)	172.69(18)	C(31)–C(32)–C(33)	174.2(6)
C(31)–Pt(1)–N(11)	175.0(2)	C(42)–C(41)–Pt(1)	176.0(5)
C(41)–Pt(1)–N(11)	95.61(19)	C(41)–C(42)–C(43)	178.1(6)

The Pt(II) complexes **Pt–PBE–Ph** and **Pt–PBPh–Py** (Figs. 5 and 6) have essentially square planar coordination geometries, with the biggest distortion from an ideal geometry arising from the limited bite angle of the chelating PB ligand (*ca.* 78° in each case). In these complexes the shortening of the Pt–N(benzimidazole) distance compared to the Pt–N(pyridyl) distance is barely significant. The Pt–C distances are likewise equivalent within the uncertainty limits so there is no obvious *trans* effect arising from the electronic inequivalence between the pyridyl and benzimidazolyl donors. The C≡C bonds have distances of 1.21–1.22 Å, in obvious contrast to the immediately following C–C single bonds (1.43–1.45 Å). The torsion angle between the pyridyl and benzimidazolyl units is 3° for **Pt–PBE–Ph** and 1° for **Pt–PBPh–Py**. As in the above cases, the formally double C=N bond within the five-membered ring of the benzimidazolyl unit is the shortest bond length in the PB ligand, at 1.331(4) Å for **Pt–PBPh–Py** and 1.341(6) Å for **Pt–PBE–Ph**, although the effect is not as marked as it is in the Re(I) and Ru(II) complexes described above. In **Pt–PBPh–Py**, the pendant phenyl ring makes an angle of 89.9° with the benzimidazole mean plane. In **Pt–PBE–Ph** adjacent near-planar units stack in pairs such that there is an axial Pt···Pt contact of 3.374 Å [Fig. 5(b)]; in **Pt–PBPh–Py** the adjacent pairs are stacked in an 'offset' manner so that there are no obvious axial Pt···Pt interactions [Fig. 6(b)].

Absorption and luminescence properties

Electronic spectra of the complexes are summarised in Table 3. In general, the lowest-energy absorption in each case is the metal-to-ligand charge transfer (MLCT) transition which is characteristic of these Re(I),[16] Ru(II)[17] and Pt(II)[18] chromophores with diimine ligands. For the Re(I) complexes these occur at ≈400 nm and are of relatively low intensity, being obscured in some cases by the more intense and sharper transitions associated with aromatic pendant groups such as anthracene and pyrene. For the Pt(II) series of complexes these MLCT transitions are more intense and clearly defined, and lie between 396 and 411 nm. For the Ru(II) series, the MLCT transition is at lower energy (459 nm). In all cases, the energies of these MLCT transitions are very similar to those observed for the analogous 2,2′-bipyridine complexes.[16–18]

Luminescence spectra of all complexes were recorded in air-equilibrated CH_2Cl_2 at ambient temperature (see Table 4). The Re(I) complexes showed only weak luminescence in every case, but the origin of the luminescence varied between different complexes. In two cases (**Re–PBN**, **Re–PBPh** and **Re–PBF**) the broad, unstructured emission band at 620–640 nm, with a quantum yield of *ca.* 10^{-3}, is typical of the weak luminescence from the ^{3}MLCT level of the Re–diimine chromophore, with luminescence parameters comparable to those of $[Re(bpy)(CO)_3Cl]$ under the same conditions.[16] Similar emission spectra were obtained at a range of different excitation wavelengths, with (in the case of **Re–PBN**) no trace of any naphthalene-based luminescence appearing at any excitation wavelength, indicating complete energy transfer from the singlet excited state of the naphthalene chromophore to the metal centre, resulting in ^{3}MLCT luminescence.

For **Re–PBA** and **Re–PBPyr**, however, excitation into the MLCT transition at ≈400 nm gives no detectable Re-based luminescence; in contrast, excitation of the sharp absorption

Table 3 Absorption spectra of the complexes (CH_2Cl_2, room temperature)

Complex	λ/nm ($10^{-3}\varepsilon$/M^{-1} cm^{-1})
Pt–PBPh–Py	396 (7.8),[a] 347 (17), 332 (19), 305 (40), 246 (34)
Pt–PBPh–CF_3	402 (8.4),[a] 348 (20), 330 (20), 294 (43), 245 (29)
Pt–PBE–CF_3	400 (8.5),[a] 348 (21), 332 (21), 293 (43), 244 (29)
Pt–PBE–Ph	409 (7.3),[a] 349 (19), 331 (21), 295 (sh), 265 (35), 248 (35)
Pt–PBF–Ph	414 (6.8),[a] 346 (16), 328 (sh), 295 (sh), 264 (35), 250 (34)
Pt–PBN–Ph	411 (7.2),[a] 349 (18), 332 (20), 267 (40), 247 (38)
Pt–PBPh–Ph	411 (7.3),[a] 348 (18), 330 (21), 264 (35), 248 (35)
Re–PBPh	387 (4.2),[a] 343 (19), 328 (20), 239 (22)
Re–PBN	388 (4.1),[a] 343 (18), 328 (19), 276 (13)
Re–PBA	393 (12), 373 (14), 346 (20), 336 (20), 258 (160)
Re–PBF	394 (3.9),[a] 342 (18), 327 (20), 239 (21)
Re–PBPyr	≈400 (sh),[a] 347 (58), 331 (48), 317 (29), 278 (48), 267 (31), 244 (87)
Ru–PBF	459 (15),[a] 339 (sh), 321 (sh), 289 (67), 244 (33)
Ru–PBA	459 (14),[a] 393 (9.2), 372 (10), 323 (sh), 290 (62), 257 (132)
Ru–PBPyr	459 (16),[a] 347 (58), 330 (52), 317 (38), 290 (69), 278 (76), 267 (40), 244 (97)
Ru–PBN	459 (15),[a] 340 (sh), 320 (sh), 289 (70), 244 (36)

[a] Lowest-energy MLCT transition.

bands associated with the anthracene or pyrene units in the UV region gives very weak, structured luminescence ($\phi \approx 10^{-4}$) from these aromatic units, centred at 380 nm for pyrene and 418 nm for anthracene. The contrast between the two types of luminescence behaviour is shown in Fig. 7. The absence of metal-based luminescence in these complexes can be ascribed to quenching of the Re-centred ^{3}MLCT excited state by the lower-lying triplet state of the anthracene or pyrene units. From the onset of luminescence at the high-energy end of the luminescence spectrum of **Re–PBN** and **Re–PBP** (*i.e.* the 0–0 transition between electronically excited and ground states) at ≈550 nm, the ^{3}MLCT energy available to the Re chromophore in these complexes is estimated to be 18200 cm^{-1}; the triplet energies of pyrene and anthracene are *ca.* 16600 cm^{-1} (ref. 19*a*) and 14500 cm^{-1} (ref. 16*c*) respectively, so such energy transfer is thermodynamically favourable, and has been observed by Schanze *et al*. in Re$^{\text{I}}$(bpy)/anthracene dyads.[16c] The observation of normal Re-based luminescence in **Re–PBN**, in which the naphthalene triplet energy is much higher than that of the metal ^{3}MLCT state and therefore cannot quench the metal-based luminescence, confirms this. Fig. 8 illustrates the approximate energy levels for the contrasting cases of **Re–PBN** and **Re–PBA**; the energies of the ^{1}MLCT and ^{3}MLCT Re states are taken from the absorption and luminescence spectra of **Re–PBN**.

In **Re–PBA**, the initially generated ^{1}An level, which has a similar energy to the ^{1}MLCT state of the Re centre, transfers its excitation energy to the metal centre. This may in principle

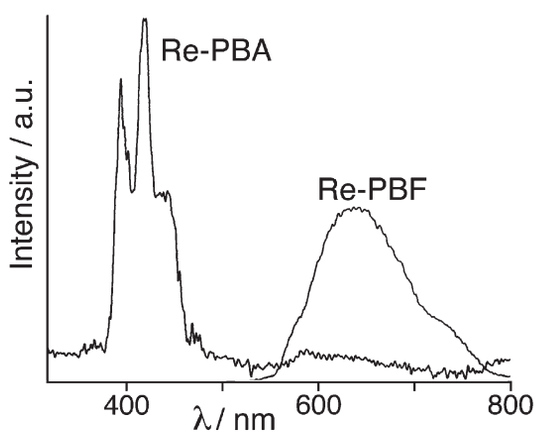

Fig. 7 Luminescence spectra of **Re–PBA** and **Re–PBF** (CH_2Cl_2, room temperature).

Table 4 Luminescence properties of the complexes (CH_2Cl_2, room temperature)

Complex	λ_{em}[a]/nm	τ/ns	ϕ[b]
Pt–PBPh–Py	553	404	0.054
Pt–PBPh–CF_3	560	515	0.059
Pt–PBE–CF_3	556	398	0.055
Pt–PBE–Ph	595	225	0.027
Pt–PBF–Ph	605	230	0.021
Pt–PBN–Ph	597	274	0.030
Pt–PBPh–Ph	600	278	0.027
Re–PBN	623	—	~10^{-3}
Re–PBPh	620	—	~10^{-3}
Re–PBF	640	—	~10^{-3}
Re–PBA	395, 418, 440[c]	—	~10^{-4}
Re–PBPyr	400	—	~10^{-4}
Ru–PBF	645	276	0.011
Ru–PBPyr	626	356	0.011
Ru–PBA	630	232	~10^{-3}
	400, 421, 445[c]	4	
Ru–PBN	630	312	0.015

[a] Emission maxima are uncorrected. [b] Quantum yields were calculated using $[Ru(bpy)_3]^{2+}$ in aerated water ($\phi = 0.028$) as standard. [c] Anthracene-based luminescence.

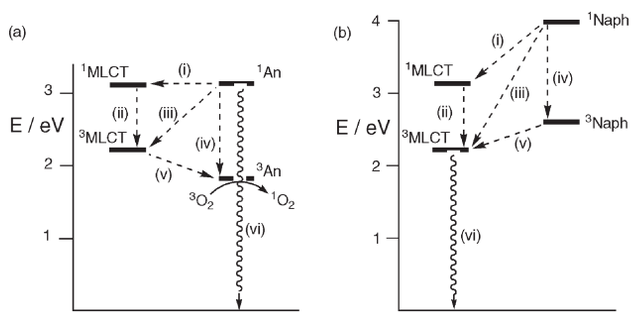

Fig. 8 Energy-level diagram for (a) **Re–PBA** and (b) **Re–PBN**. For details see main text.

occur either to the ^{1}MLCT state [spin-allowed; process (i) in Fig. 8(a)] followed by inter-system crossing to the ^{3}MLCT state [process (ii)], or directly to the ^{3}MLCT state [process (iii), a spin-forbidden process facilitated by the high spin–orbit coupling of the Re atom]. The ^{3}MLCT state then undergoes a second energy-transfer step to give the lower-lying ^{3}An state [process (v)], which is efficiently quenched by dissolved oxygen. An exactly similar double energy-transfer sequence (aromatic singlet → metal ^{3}MLCT → aromatic triplet) has been proposed recently to account for the behaviour of $[Ru(bpy)_3]^{2+}$/pyrene[19] and $[Ru(bpy)_3]^{2+}$/anthracene[20] dyads; the same sequence of events can also be suggested for **Re–PBPyr**. The presence of very weak residual fluorescence from the pyrene and anthracene units [Fig. 8(a), process (vi)] in **Re–PBPyr** and **Re–PBA** is simply ascribable to incomplete energy transfer for the first step, possibly due to the low gradient for energy transfer; in **Re–PBN**, where the singlet excited state of the naphthalene unit is considerably higher in energy [Fig. 8(b)], no naphthalene-based emission was detected: all excitation energy from the ^{1}Naph state ends up populating the ^{3}MLCT state, with consequent Re-based emission [Fig 8(b), process (vi)].

In contrast to the Re(I) complexes, the series of Pt(II) complexes showed strong, long-lived luminescence with quantum yields and lifetimes considerably better, in some cases, than $[Ru(bpy)_3]^{2+}$ under the same conditions; as with the Re(I) complexes, the luminescence behaviour of these Pt(II)–PB complexes is generally similar to that of the 2,2′-bipyridyl analogues.[18] It is noticeable that the presence of electron-withdrawing substituents on the acetylene units ($C_6H_4CF_3$; 2-pyridyl) has a substantially beneficial effect on the photophysical properties of the complexes, with higher energy for the luminescence, higher quantum yields and longer lifetimes (see Table 4). This is ascribable to the fact that decreased π-donor/increased π-acceptor for the acetylide

ligands will strengthen the ligand field at the metal and cause the d(π) orbitals to drop in energy. Consequently, the luminescence maxima for these complexes (550–560 nm) are at significantly higher energy than the others which do not have electron-withdrawing substituents (emission maxima *ca.* 600 nm). The higher energy of the ^{3}MLCT state results in more intense luminescence, in accordance with the energy-gap law, as higher overtones of molecular vibrations will be needed to effect non-radiative decay. For **Pt–PBN–Ph**, no luminescence from the naphthyl unit was detected, indicating (as for **Re–PBN**) efficient energy transfer from the aromatic antenna unit to the metal centre.

The strong beneficial effect of electron-withdrawing groups attached to the acetylide ligands prompted us to examine the effect of protonation of the pendant pyridyl residues of **Pt–PBPh–Py** on the luminescence. These experiments were performed in MeCN to avoid the possibility of the protonated complex precipitating from CH_2Cl_2; the result is shown in Fig. 9. In MeCN the MLCT absorption maximum is at 390 nm, slightly blue-shifted compared to the situation in CH_2Cl_2. On bubbling HCl vapour to the solution there is a substantial change in the absorption spectrum in the 300–400 nm region (Fig. 9(a)), with the MLCT transition moving to 367 nm and approximately trebling in intensity, in agreement with expectations based on the acetylide ligand becoming a better π-acceptor/poorer π-donor. The transition at 340 nm likewise gains substantially in intensity, although it remains at the same position. The two spectra have an iso-absorbing point at 396 nm which was used for excitation in the luminescence spectra. The luminescence maximum of **Pt–PBPh–Py** is at 545 nm, with a shoulder on the low-energy side arising from vibronic effects. Bubbling HCl vapour through the solution (Fig. 9(b)) resulted in a blue-shift of the luminescence to 516 nm, with the low-energy shoulder (now at 548 nm) being more clearly resolved, and in increase in quantum yield of about 15% relative to the non-protonated form. Clearly, protonation of the pendant pyridyl groups is increasing their electron-withdrawing ability and consequently increasing the energy and intensity of luminescent emission. This offers interesting possibilities for use of the molecules as luminescent sensors for metal ions, since coordination of the pyridyl residues to metal ions will have a similar electronic effect to protonation. Importantly, a change in the wavelength (and not just the intensity) of emission when the pyridyl residues interact with a metal cation may allow use of this complex and others like it as a ratiometric sensor for quantifying metal ions.

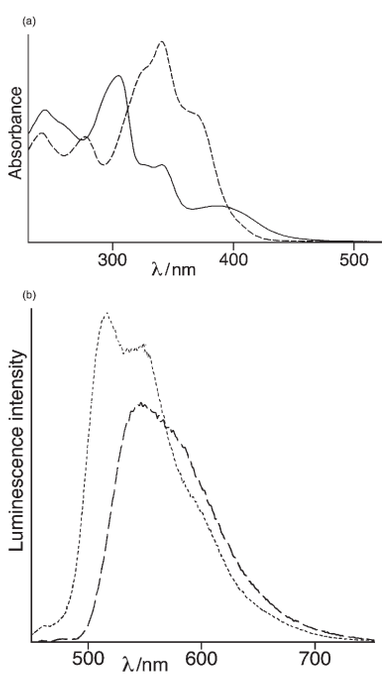

Fig. 9 Effect of protonation of the pendant pyridyl groups on the (a) absorption and (b) luminescence spectra of **PtPy–PBPh**. In (a) the solid line is the spectrum of the complex on its own; the dashed line shows the effect of protonation. In (b) the dashed line is the luminescence spectrum of the complex on its own; the dotted line shows the effect of protonation.

The **Ru–PB** complexes show in the 630–650 nm region the characteristic luminescence from the ^{3}MLCT excited state,[17] at slightly lower energies than $[Ru(bpy)_3]^{2+}$ (consistent with the reduced energy of the MLCT absorption maximum, *i.e.* 459 nm rather than 450 nm) and with reduced quantum yields (typically, ≈1%, with the exception of **Ru–PBA**; see below) and lifetimes of a few hundred nanoseconds. From the onset of the emission spectra at the high energy-end (≈570 nm), the energy of the ^{3}MLCT state for these Ru–PB chromophores can be estimated as ≈17500 cm^{-1}, which is slightly lower than the energy of the Re-based ^{3}MLCT state, the normal pattern for Re(I) and Ru(II)–diimine complexes.[16b,d]

For **Ru–PBN** and **Ru–PBPyr,** excitation at higher wavelengths—into the UV absorption bands of the pendant aromatic chromophores (at 263 or 317 nm for naphthalene and pyrene respectively)—also resulted in Ru-based luminescence but with a slightly reduced quantum yield (by ≈ 20% compared to direct excitation of the Ru–PB chromophore). Also present was very weak, almost vestigial, luminescence characteristic of the naphthalene or pyrene units in the 350–400 nm region (Fig. 10). Energy transfer from the appended organic chromophore singlet state to the Ru centre is therefore occurring with less than 100% efficiency, despite the fact that these pendant organic chromophores have singlet energies that are sufficiently high in energy to act as energy-donors, and are spatially close to the metal centre. In fact the driving force for energy transfer from ^{1}Naph and ^{1}Pyr to the metal centre should be greater than in the Re series, because the MLCT levels of the Ru chromophore are lower in energy,[16b,d] so the incompleteness of the energy transfer is surprising. In **Ru–PBPyr**, energy transfer in the other direction, from the Ru ^{3}MLCT level to the triplet pyrene level, is clearly not a significant quenching pathway since the quantum yields and lifetimes for Ru-based luminescence of **Ru–PBPyr, Ru–PBN** and **Ru–PBF** are all comparable. This is also surprising given that the Ru-based ^{3}MLCT state is expected to be higher in energy than the ^{3}Pyr state by ≈1000 cm^{-1}. We note, however, that this gradient is less than that which occurs in **Re–PBPyr**, where ^{3}MLCT(Re)→^{3}Pyr was efficient and resulted in complete quenching of the Re-based luminescence.

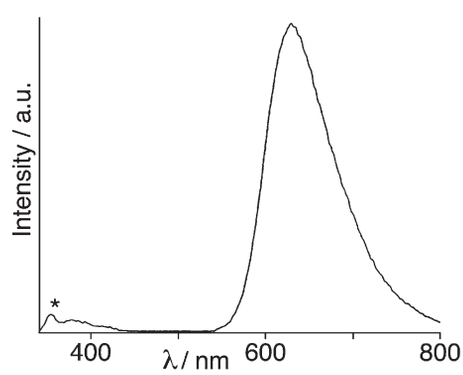

Fig. 10 Luminescence spectrum of **Ru–PBPyr** showing weak residual pyrene-based luminescence (*) in addition to the ^{3}MLCT luminescence.

Similar behaviour (incomplete energy transfer between metal and organic chromophores) occurs when anthracene is the pendant chromophore, in **Ru–PBA**. In this complex the metal-centred luminescence at 630 nm is an order of magnitude less intense than in the other Ru(II) complexes and, depending on the excitation wavelength, structured fluorescence from the anthracene singlet excited state can also be seen between 390 and 450 nm (Fig. 11). Excitation spectra recorded monitoring the Ru-based emission at 630 nm, and the anthracene-based emission at 420 nm, show quite clearly distinct absorption features which are mutually independent (Fig. 12). Thus, anthracene-based

luminescence occurs only on irradiation into the strong anthracene absorption at 260 nm and the weaker absorptions between 340 and 400 nm. Conversely, Ru-based luminescence only occurs on excitation into those features of the absorption spectrum at 270–350 nm, and at 459 nm, which are characteristic of the Ru–tris(diimine) chromophore. The two luminescent states (^{1}An and ^{3}MLCT) are only weakly interacting, with energy transfer from the anthracene singlet excited state to the Ru centre being absent (since no sensitised Ru-based emission occurs following excitation of anthracene) despite the fact that it is thermodynamically favourable. The very weak anthracene luminescence nonetheless means that the ^{1}An state is substantially quenched, which can be ascribed to direct conversion to the (non-emissive) low-energy triplet state of anthracene (^{3}An) by inter-system crossing caused by the proximity of a heavy metal ion. In contrast, the anomalous weakness of the Ru-based luminescence (Table 4) can only be ascribed to (incomplete) energy transfer to the ^{3}An level (*ca.* 14500 cm^{-1}), which is not luminescent under the conditions of the experiment. Similar behaviour was also observed for **Re–PBA**, although in this case quenching of the ^{3}MLCT state by the ^{3}An state was complete rather than partial, presumably due in part to the slightly higher thermodynamic gradient in **Re–PBA** compared to **Ru–PBA**. Similar behaviour has been observed in solution for a $[Ru(bpy)_3]^{2+}$/anthracene dyad

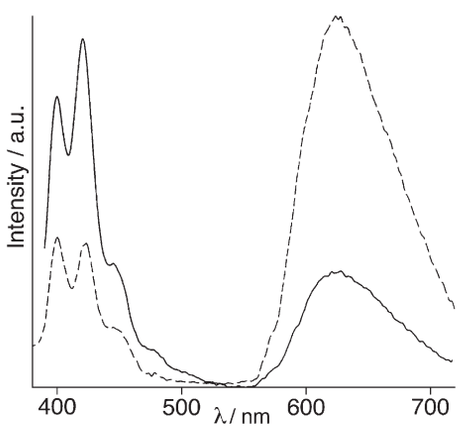

Fig. 11 Luminescence spectra for **Ru–PBA**, measured using excitation at 370 nm (solid line) and 269 nm (dashed line).

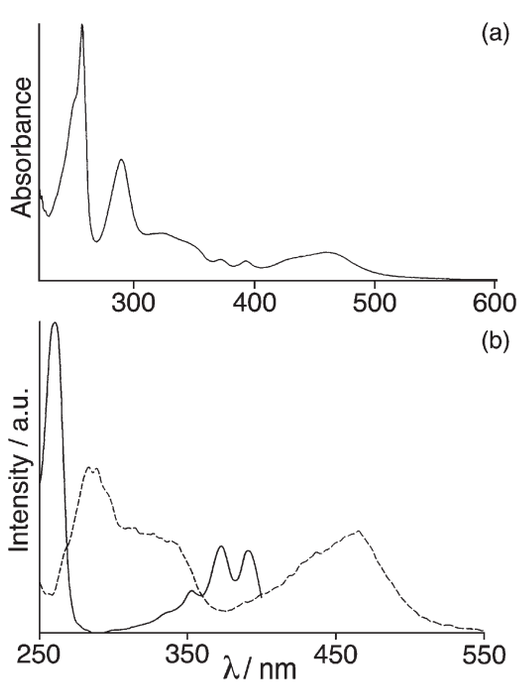

Fig. 12 (a) UV/Vis absorption spectrum of **Ru–PBA**; (b) excitation spectra of **Ru–PBA**, recorded using the anthracene-based emission at 400 nm (solid line) and the ruthenium-based emission at 630 nm (dashed line).

in which luminescence from both components was completely quenched.[20]

Time-resolved measurements on **Ru–PBA** showed that the Ru-based luminescence, although of low intensity, is still reasonably long-lived with τ = 232 ns. The very weak anthracene-based luminescence (monitored at 400 nm) is much shorter-lived with a lifetime of about 4 ns, much less than the value of *ca.* 11 ns which is typical for unquenched anthracene fluorescence.[21] This, together with the very low intensity, confirms a high degree of quenching of the anthracene excited state.

To summarise this section, we can say two things. Firstly, the metal–PB chromophores show luminescence properties from their ^{3}MLCT excited states which are comparable in energy, intensity and lifetime to those of the better-known metal–bipyridyl chromophores. Secondly, the complexes with pendant aromatic chromophores, particularly anthracene and pyrene, show complex photophysical behaviour due to inter-component energy-transfer processes between the organic and metal-PB chromophores, which are more efficient (in both directions) for the Re series than the Ru series. The slightly lower energies of the MLCT states for the Ru series compared to the Re series may explain why energy transfer from the metal ^{3}MLCT state to the ^{3}Pyr or ^{3}An state is incomplete or absent in the Ru series, because the gradient is reduced. However, this ordering of energy levels should result in faster energy transfer in the other direction, from ^{1}Pyr or ^{1}An to the metal centre, which is clearly not the case; this energy transfer is also poorer for the Ru series, being incomplete in **Ru–BPPyr** and absent in **Ru–PBA.**

A plausible explanation for this is the different spatial localisation of the MLCT states in the Ru and Re series. For the Re series there is only one diimine ligand, the PB unit; the ^{1}MLCT and ^{3}MLCT excited states must necessarily involve this ligand. Accordingly the effective distance for energy transfer between the MLCT states and organic chromophores is small, since the pyrene, anthracene and naphthalene units are directly attached to the PB ligand with only a single atom (methylene) spacer. In the Ru series, however, there are two different types of diimine ligand; the PB unit and the bipyridyl ligands. If the MLCT states involve the bipyridyl ligands and not the PB ligand, then they will be localised in a region of space much further away from the appended organic chromophore, giving a greater effective distance for energy transfer between the components. In the original paper describing $[Ru(bpy)_2(PB)]^{2+}$ complexes,[4] Haga pointed out that benzimidazole is a slightly better π-donor/poorer π-acceptor than bipyridine, and our electrochemical data (described below) confirm that bpy is a slightly better electron-acceptor than PB in a homologous pair of complexes. This means that, in the mixed-ligand series of Ru complexes, the lowest-energy ^{3}MLCT state should indeed be localised on one of the bipyridyl ligands rather than the PB unit, and the effective energy-transfer distance to or from the organic chromophores will be much larger than in the Re series. An exactly similar effect was described recently by Constable *et al.*, in which the rate of energy transfer between $\{Ru(terpy)_2\}^{2+}$ and $\{Os(terpy)_2\}^{2+}$ units depended on whether the Ru-based ^{3}MLCT excited state involved the terpyridine ligand closer to the Os(II) centre or the one which was more remote.[22]

Redox properties

The redox properties of representative members of each series were measured by cyclic voltammetry in CH_2Cl_2 solution using a scan rate of 0.5 V s^{-1} (Fig. 13). **Ru–PBN** showed a reversible one-electron process at +0.86 V *vs.* Fc/Fc$^+$ which we ascribe to the Ru(II)/Ru(III) couple (*cf.* +0.89 V for $[Ru(bpy)_3]^{2+}$ under the same conditions). There are also two reversible one-electron processes at −1.72 and −1.98 V, clearly ligand-based; the first two reductions of $[Ru(bpy)_3]^{2+}$ occur at −1.72 and −1.92 V *vs.* Fc/Fc$^+$. Given the fact that the PB unit is a slightly poorer π-acceptor than bpy,[4] it is likely that these two reductions are both bpy-centred. Similar results were found for **Ru–PBA** (metal-based

process, +0.83 V; ligand-based processes, −1.76 and −1.95 V *vs.* Fc/Fc^+). In this case however the ligand-based processes showed weak return waves and are hence irreversible. In addition, for **Ru–PBA** a second anodic process was present at +1.03 V, which was the same intensity as the others, *i.e.* a one-electron process. It was not however fully reversible, with the return wave being smaller than the outward wave. This process can be assigned to oxidation of the pendant anthracene unit to its radical cation (irreversible oxidation of anthracene to its radical cation in CH_2Cl_2 has been reported to occur at +1.04 V *vs.* Fc/Fc^+).[23] In **Ru–PBPyr** the Ru(II)/Ru(III) couple is obscured by an electrode absorption/desorption process, but two ligand-based couples are at −1.70 and −1.97 V, with the first being reversible but the second being broad (peak-peak separation, ≈ 200 mV).

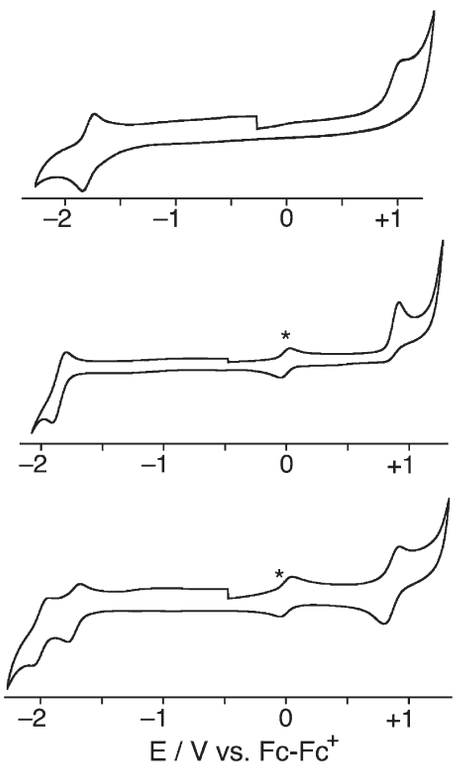

Fig. 13 Cyclic voltammograms of (a) **Pt–PBE–Ph**; (b) **Re–PBPh**; (c) **Ru–PBN** in CH_2Cl_2 at a scan rate of 500 mV s^{-1} with a Pt disk working electrode. * denotes the redox couple of ferrocene which was added as an internal reference.

Members of the Pt(II) series all showed a reversible one-electron couple at negative potential characteristic of a ligand-based reduction; the potentials are −1.83, −1.80 and −1.77 V *vs.* Fc/Fc^+ for **Pt–PBPh–Py**, **Pt–PBE–Ph** and **Pt–PBE–CF_3**, respectively. Wholly irreversible oxidations are present between +0.8 and +1 V *vs.* Fc/Fc^+. For comparison, members of the Pt(diimine)$(CCR)_2$ series show a ligand-based reduction on the bipyridyl or phenanthroline unit at *ca.* −1.7 to −1.8 V *vs.* Fc/Fc^+, and (sometimes) an irreversible oxidation at around +0.8 V *vs.* Fc/Fc^+.[18a] It is clear from this, as from the measurements on the Ru series, that the PB ligands confer very similar electronic properties on their complexes to bipyridine ligands.

Members of the Re(I) series showed irreversible Re(I)/Re(II) processes at positive potentials, and ligand-based processes at negative potentials which are reversible at high scan rates (500 mV s^{-1}). This behaviour is characteristic of related Re(I)–bipyridyl complexes.[16a] For **Re–PBPh** the metal-based couple is completely irreversible (no return wave); the peak of the outward wave occurs at +1.96 V *vs.* Fc/Fc^+. The reversible ligand-centred couple occurs at −1.84 V. **Re–PBPyr** behaves similarly, with an irreversible oxidation showing evidence of electrode adsorption, but a ligand-centred couple at −1.82 V. For **Re–PBA** the metal-based irreversible process is at +0.96 V, and this time the ligand-based process is also irreversible with the peak potential on the outward scan being −1.94 V. The irreversible anthracene-based oxidation was also present, with the peak potential of the outward wave being at +1.33 V.

Importantly, the PB-based redox couple of members of the Re(I) series occur at slightly more negative potentials (by *ca.* 100 mV) than the bpy-based redox couple of $[Re(bpy)(CO)_3Cl]$,[16a] which allows a direct comparison between the electronic properties of coordinated PB *vs.* bpy ligands. These electrochemical data confirm that PB is a poorer π-acceptor than bpy (*cf.* Haga's initial paper).[4] This supports the suggestion that in the Ru-based complexes the MLCT excited states are localised on the bpy ligands rather than the PB ligand, which accounts for the poor energy transfer between the MLCT states and the pendant aromatic chromophores, as described above.[24]

Conclusions

The main general conclusion to arise from this work is that PB-based ligands provide redox and photophysical properties in their complexes which are generally comparable to those obtained with the much better studied 2,2′-bipyridyl ligands, although with slightly lower ^{3}MLCT energies. The ease of functionalisation of the PB units compared to bipyridine provides a considerable advantage for synthesis of multi-chromophoric complexes. Two further points of interest also arose. Firstly, the efficiency of photoinduced energy transfer between the metal centre and the pendant organic luminophore appears to depend on the spatial localisation of the ^{3}MLCT excited state of the metal centre. If the ^{3}MLCT excited state involves the PB unit to which the organic luminophore is connected (as in the Re series), energy transfer occurs over a short distance and is virtually quantitative; if however the ^{3}MLCT excited state is localised on an ancillary (bpy) ligand away from the PB unit and its pendant luminophore, the inter-component energy transfer occurs over a larger distance and is incomplete. Secondly, the Pt series showed particularly intense and long-lived luminescence, especially with electron-withdrawing substituents on the acetylide ligands. With 2-pyridyl groups on the acetylides, protonation/deprotonation of these pyridyl units provides a reversible way of increasing or decreasing the electron-withdrawing effect of the substituents and hence modulating the luminescence properties of the complex.

Acknowledgements

We thank the Royal Society/NATO for a post-doctoral fellowship (N. M. S.) and EPSRC for a post-doctoral fellowship (Z. R. B.) and a PhD studentship (T. L. E.).

References

1 (*a*) V. Balzani and F. Scandola, *Supramolecular Photochemistry*, Ellis Horwood, Chichester, UK, 1991; (*b*) V. Balzani and F. Scandola, in *Comprehensive Supramolecular Chemistry*, vol. 10 (ed. D. N. Reinhoudt), Elsevier, Oxford, UK, 1996, p. 687; (*c*) C. Kaes, A. Katz and M. W. Hosseini, *Chem. Rev.*, 2000, **100**, 3553; (*d*) V. Balzani, A. Juris, M. Venturi, S. Campagna and S. Serroni, *Chem. Rev.*, 1996, **96**, 759.
2 T. R. Harkins, J. L. Walter, O. E. Harris and H. Freiser, *J. Am. Chem. Soc.*, 1956, **78**, 260; B. Chiswell, F. Lions and B. S. Morris, *Inorg. Chem.*, 1964, **3**, 110.
3 B. De Castro, C. Freire, D. Domingues and J. Gomes, *Polyhedron*, 1991, **10**, 2541; M. Maekawa, M. Munakata, T. Kuroda-Sowa and K. Hachiya, *Inorg. Chim. Acta*, 1994, **227**, 137; M. M. H. Khalil, S. A. Ali and R. M. Ramadan, *Spectrochim. Acta, Part A*, 2001, **57**, 1017; R. Boca, P. Baran, L. Dlhán, J. Sima, G. Wiesinger, F. Renz, U. El-Ayaan and W. Linert, *Polyhedron*, 1997, **16**, 47.
4 M. Haga, *Inorg. Chim. Acta*, 1983, **75**, 29.
5 M. Haga and A. Tsunemitsu, *Inorg. Chim. Acta*, 1989, **164**, 137.
6 L. J. Charbonnière, A. F. Williams, C. Piguet, G. Bernardinelli and E. Rivara-Minten, *Chem. Eur. J.*, 1998, **4**, 485; C. Piguet, G. Bernardinelli and G. Hopfgartner, *Chem. Rev.*, 1997, **97**, 2005.
7 (*a*) H. Yi, J. A. Crayston and J. T. S. Irvine, *Dalton Trans.*, 2003, 685; (*b*) K. Wang, L. Huang, L. Gao, L. Jin and C. Huang, *Inorg. Chem.*, 2002, **41**, 3353; (*c*) B. H. Kim, D. N. Lee, H. J. Park, J. H. Min, Y. M. Jun, S. J. Park and W.-Y. Lee, *Talanta*, 2004, **62**, 595.

8 M. D. Hossain, M. Haga, B. Gholamkhass, K. Nozaki, M. Tsushima, N. Ikeda and T. Ohno, *Collect Czech. Chem. Commun.*, 2001, **66**, 307; M. M. Ali, H. Sato, M. Haga, K. Tanaka, A. Yoshimura and T. Ohno, *Inorg. Chem.*, 1998, **37**, 6176; B. Gholamkhass, K. Nozaki and T. Ohno, *J. Phys. Chem. B*, 1997, **101**, 9010.
9 K. A. Reeder, E. V. Dose and L. J. Wilson, *Inorg. Chem.*, 1978, **17**, 1071.
10 L. Huang, K. Z. Wang, C. H. Huang, F. Y. Li and Y. Y. Huang, *J. Mater. Chem.*, 2001, **11**, 790.
11 B. P. Sullivan, D. J. Salmon and T. J. Meyer, *Inorg. Chem.*, 1978, **17**, 3334.
12 G. M. Sheldrick: *SADABS, A program for absorption correction with the Siemens SMART area-detector system*, University of Göttingen, 1996.
13 G. M. Sheldrick: *SHELXS-97 and SHELXL-97 programs for crystal structure solution and refinement*, University of Göttingen, 1997.
14 T. Rajendran, B. Manimaran, F. Y. Lee, G. H. Lee, S. M. Peng, C. C. Wang and K. L. Lu, *Inorg. Chem.*, 2000, **39**, 2016; N. M. Shavaleev, Z. R. Bell and M. D. Ward, *J. Chem. Soc., Dalton Trans.*, 2002, 3925; N. M. Shavaleev, Z. R. Bell, G. Accorsi and M. D. Ward, *Inorg. Chim. Acta*, 2003, **351**, 159; N. M. Shavaleev, A. Barbieri, Z. R. Bell, M. D. Ward and F. Barigelletti, *New J. Chem.*, 2004, **28**, 398.
15 D. P. Rillema, D. S. Jones and H. A. Levy, *J. Chem. Soc., Chem. Commun.*, 1979, 849.
16 (*a*) L. A. Worl, R. Duesing, P. Chen, L. Della Ciana and T. J. Meyer, *J. Chem. Soc., Dalton Trans.*, 1991, 849; (*b*) D. A. Bardwell, F. Barigelletti, R. L. Cleary, L. Flamigni, M. Guardigli, J. C. Jeffery and M. D. Ward, *Inorg. Chem.*, 1995, **33**, 2438; (*c*) K. S. Schanze, D. B. MacQueen, T. A. Perkins and L. A. Cabana, *Coord. Chem. Rev.*, 1993, **122**, 63; (*d*) N. Armaroli, G. Accorsi, D. Felder and J.-F. Nierengarten, *Chem. Eur. J.*, 2002, **8**, 2314.
17 A. Juris, V. Balzani, F. Barigeletti, S. Campagna, P. Belser and A. von Zelewsky, *Coord. Chem. Rev.*, 1988, **84**, 85.
18 (*a*) M. Hissler, M. Connick, D. K. Geiger, J. E. McGarrah, D. Lipa, R. J. Lachiotte and R. Eisenberg, *Inorg. Chem.*, 2000, **39**, 447; (*b*) E. C. Whittle, J. A. Weinstein, M. W. George and K. S. Schanze, *Inorg. Chem.*, 2001, **40**, 4053; (*c*) S. C. Chan, M. C. W. Chan, Y. Wang, C.-M. Che, K. K. Cheung and N. Y. Zhu, *Chem. Eur J.*, 2001, **7**, 4180; (*d*) S. L. James, M. Younus, P. R. Raithby and J. Lewis, *J. Organomet. Chem.*, 1997, **543**, 233.
19 (*a*) W. E. Ford and M. A. J. Rogers, *J. Phys. Chem.*, 1992, **96**, 2917; (*b*) A. Harriman, M. Hissler, A. Khatyr and R. Ziessel, *Chem. Commun.*, 1999, 735; (*c*) A. F. Morales, G. Accorsi, N. Armaroli, F. Barigelletti, S. J. A. Pope and M. D. Ward, *Inorg. Chem.*, 2002, **41**, 6711; (*d*) N. D. McClenaghan, F. Barigelletti, B. Maubert and S. Campagna, *Chem. Commun.*, 2002, 602.
20 G. J. Wilson, A. Launikonis, W. H. F. Sasse and A. W.-H. Mau, *J. Phys. Chem.*, 1997, **101**, 4860.
21 (*a*) G. Greiner, *J. Photochem. Photobiol. A*, 2000, **137**, 1; (*b*) J. H. Clements and S. E. Webber, *J. Phys. Chem. B*, 1999, **103**, 9366.
22 E. C. Constable, R. W. Handel, C. E. Housecroft, A. F. Morales, L. Flamigni and F. Barigelletti, *Dalton Trans.*, 2003, 1220.
23 A. Matsuura, T. Nishinaga and K. Komatsu, *Tetrahedron Lett.*, 1997, **38**, 3427.
24 One of the referees suggested the possibility that the differences between inter-component energy transfer in the Re and Ru series could be due in part to conformational effects, because the orientation of the aromatic chromophore with respect to the metal–tris(chelate) centre would affect orbital interactions between them. Whilst this is in principle possible we do not think that it is a factor here, because the ligand conformations do not (according to crystal structures) differ much between the series. For example, the pendant aromatic unit is essentially perpendicular to the PB chelating unit in both the Ru and the Re series (Figs. 3 and 4). The explanation based on electronic differences between bpy and PB, however, explains nicely why energy transfer between aromatic and metal complex chromophores is complete (or near-complete) for all members of the Re series, whereas it is clearly inefficient for all members of the Ru series.